

From Homochiral Clusters to Racemate Crystals: Viable Nuclei in 2D Chiral Crystallization

Johannes Seibel,[†] Manfred Parschau,[†] and Karl-Heinz Ernst*,^{†,‡}

[†]Empa, Swiss Federal Laboratories for Materials Science and Technology, 8600 Dübendorf, Switzerland

[‡]Department of Chemistry, University of Zurich, 8057 Zürich, Switzerland

S Supporting Information

ABSTRACT: The quest for enantiopure compounds raises the question of which factors favor conglomerate crystallization over racemate crystallization. Studying nucleation and crystal growth at surfaces with submolecular-resolution scanning tunneling microscopy is a suitable approach to better understand intermolecular chiral recognition. Racemic heptahelicene on the Ag(100) surface shows a transition from homochiral nuclei to larger racemic motifs, although the extended homochiral phase exhibits higher density. The homochiral–heterochiral transition is explained by the higher stability of growing nuclei due to a better match of the molecular lattice to the substrate surface. Our observations are direct visual proof of viable nuclei.

How molecular structure is recognized by other molecules is one of the most fundamental questions in chemistry. The process of homochiral or heterochiral aggregation of molecules, for example, is assumed to have been important in the prebiotic origin of life.^{1,2} In three dimensions, chiral molecules form either homochiral crystals, i.e., each single crystal containing only one of the two enantiomers, or racemic crystals, containing both enantiomers.³ Racemic crystals outnumber conglomerates by far, and there have been numerous attempts to explain this fact. Based on eight examples, for instance, Liebisch reported in 1895 (in a paper solely authored by Wallach) that enantiomers are more densely packed in racemic crystals than in enantiopure crystals.⁴ This conclusion, mistakenly coined as Wallach's rule,⁵ has been substantiated later for resolvable enantiomers,⁵ but was questioned for amino acids.⁶ Brock et al. proposed that a kinetic bias should favor racemate crystallization, because of the equal probability of arrival of the "wrong" enantiomer to the nucleus.⁵ Although more than 165 years have passed since Pasteur's seminal discovery of conglomerate crystallization, not much is understood about this phenomenon at the microscopic level, in part, because structures of crystal nuclei in solution or melt are hardly accessible.

Heterogeneous nucleation at surfaces is strongly favored over homogeneous nucleation in solution. Hence, the structure of the host surface should play an important role, especially for the outcome of optical resolution of chiral molecules. Consequently, studying the nucleation and growth of chiral molecules at surfaces is a promising approach to shine more light onto the chiral discrimination during conglomerate or racemate

crystallization.⁷ Aside from crystallization,⁸ how chiral information can propagate on a surface from a single molecule into supramolecular chiral structures is also relevant for technological processes such as performance of liquid crystals⁹ and heterogeneous enantioselective catalysis.¹⁰

By using scanning tunneling microscopy (STM), we have shown recently that pure enantiomers as well as racemic (*rac*) mixtures of the helically shaped aromatic heptahelicene ([7]H, C₃₀H₁₈, Figure 1) basically generate identical 2D crystal

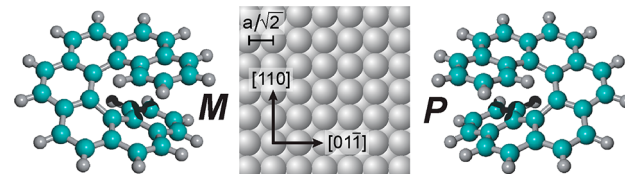


Figure 1. Ball-and-stick molecular models for *M*- and *P*-heptahelicene ([7]H, C₃₀H₁₈) and model of the Ag(100) surface (middle). The high-symmetry directions are indicated. The shortest interatomic distance is 2.89 Å ($a = 4.09$ Å).

structures on the 3-fold symmetric fcc(111) surfaces of Cu, Ag, and Au.¹¹ The racemate notably forms a previously well-characterized heterochiral *M-P*-zigzag row motif.^{12,13} In contrast, the 4-fold-symmetric Cu(100) surface exclusively favors conglomerate crystallization, and therefore homochiral domains.¹⁴ As stable nuclei, homochiral quadruplets were identified on Cu(100), dominating as structural motifs throughout the crystal growth. In all cases [7]H was found to be adsorbed with the terminal phenanthrene group parallel to the surface.

There are only a few examples of coexistence of 2D conglomerate and racemate crystals as well as phase transitions from one to the other with increasing surface coverage. These cases were mainly concerned with planar polar prochiral molecules.^{15–19} Based on thermal stability, a conglomerate–racemate transition has previously been reported for tartaric acid on Cu(110).²⁰ Here we show with STM that [7]H initially nucleates into homochiral quadruplets on Ag(100), but then grows racemic zigzag rows with many molecules. Our results are therefore a direct visualization of preferred crystallization due to more viable nuclei.

Received: March 3, 2015

Published: June 12, 2015

Racemic [7]H was purchased from Chiracon GmbH. Metal substrate preparation and enantioseparation of [7]H have been described previously.¹³ The helicenes were deposited by sublimation from a cell held at 160 °C. The Ag(100) crystal was kept at room temperature during deposition. The sample was then slowly cooled to allow 2D nucleation and growth. All STM images were taken under ultrahigh vacuum conditions ($p < 5 \times 10^{-10}$ mbar) with a variable-temperature STM (Omicron Nanotechnology) at around 60 K. Binding energies of molecular dimers, tetramers, pentamers, and hexamers were calculated by AMBER force field geometry optimization with the HyperChem 7.1 package.

Figure 2 shows a series of STM images for racemic [7]H on Ag(100) with increasing coverage. At very low coverage only quadruplets are observed. Zigzag rows running parallel to the two high-symmetry directions of the substrate appear already at slightly higher coverage. With further coverage increase the zigzag rows grow in length and a few more quadruplets emerge. However, only the zigzag rows grow, i.e., become longer and longer with increasing coverage while the quadruplets start to disappear, until at monolayer saturation coverage only large domains of the zigzag row structure exist.

The initially formed quadruplets (Figure 2a) are homochiral and contain therefore either only *P*- or *M*-enantiomers, while the later formed zigzag rows are heterochiral. This is confirmed by studying the structure formed after deposition of the *M*-enantiomer: only one of the two enantiomorphous quadruplet types is observed. The growth leads then to only one mirror domain [Figure 3, Supporting Information (SI) Figure S1]. Interestingly, the packing density of this extended quadruplet structure is basically identical to the quadruplet structures observed for [7]H on Cu(100) and Au(111),^{11,14} namely $110.5 \text{ \AA}^2 \pm 0.5 \text{ \AA}^2$ are occupied per molecule. However, only for Cu(100) the four molecules in the unit cell occupy identical sites. Attempts to model a structure on Ag(100) with identical sites of all four molecules lead to results that are not compatible to the experimental observations (SI Figure S2). There are also heterochiral zigzag quadruplets observed after deposition of *rac*-[7]H (Figure 2d, insets), which can be easily distinguished from the homochiral quadruplets by their different alignment relative to the [110] direction (arrows).

A common observation in 2D crystals of chiral molecules is 2D enantiomorphism. That is, chirality gets transmitted at different length scales into the extended monolayer.²¹ A usual consequence is then the formation of mirror domains with the adlattice vectors aligned in an oblique angle to the underlying substrate surface.⁷ Even 2D racemate crystals may express such enantiomorphism, because of a mirror breaking relative alignment of both enantiomers. Here, however, the zigzag rows of the closed-packed racemate structure run parallel to the highly symmetric surface directions and enantiomorphism is not expressed by opposite tilt angles. Nevertheless, there are still mirror domains present, differing only in sequence of both enantiomers. That is, an *M-P-M-P* sequence, for example, is enantiomorphous to a *P-M-P-M* sequence. Two mirror domains in line with the same substrate direction, but with opposite enantiomer sequence, are shown in Figure 4. The handedness in a single molecule is judged by the clockwise or counterclockwise sequence of bright lobes in the STM appearance, as successfully applied for helicenes before.^{11,14,22} For constant current images, a brighter feature means larger height. The difference in lobe brightness of a single molecule decreases in either a clockwise or counterclockwise sequence, thus revealing

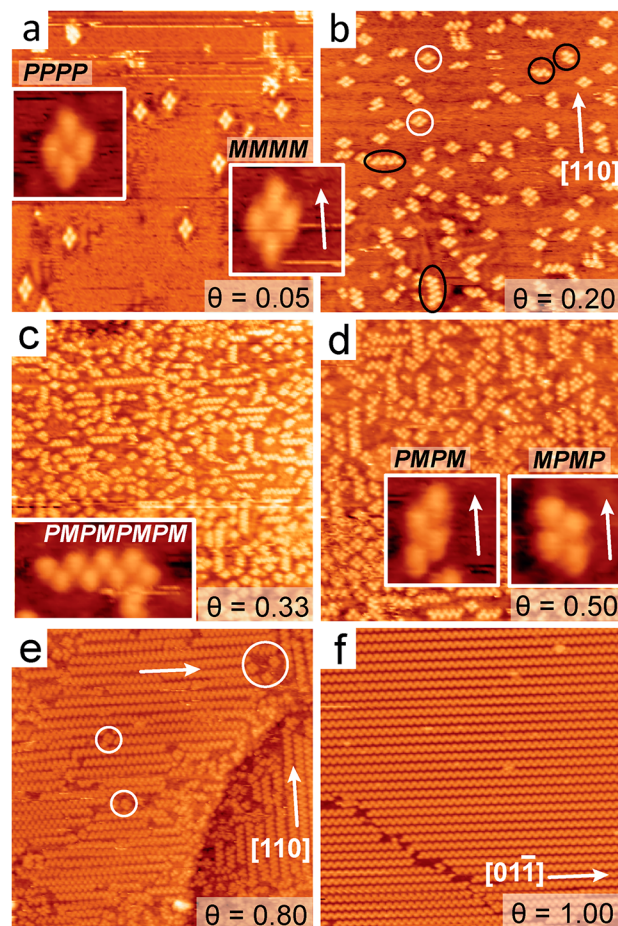


Figure 2. STM images taken at different coverages after *rac*-[7]H deposition on Ag(100). High-symmetry directions are indicated by white arrows. At the coverage of $\theta = 0.05$ (i.e., 5% of a closed-packed monolayer) only homochiral quadruplets are observed on the surface (a). At 20% zigzag rows start to form (b, black ellipses and inset in c), coexisting with quadruplets (white circles). At intermediate coverages longer zigzag rows coexist with quadruplets (c, d). At $\theta = 0.8$ the zigzag rows dominate and only few quadruplets are left at defects (e). In the saturated monolayer all quadruplets disappeared and the single domain size increased substantially (f). The insets (all taken from image b) show homochiral and heterochiral quadruplets (labeled PPPP, MMMM, PMPM, and MPMP, respectively) and a PM zigzag row (2c). Measurement parameters: (a) $50 \text{ nm} \times 50 \text{ nm}$, -2.84 V , 31 pA , insets $5 \text{ nm} \times 5 \text{ nm}$; (b) $45 \text{ nm} \times 45 \text{ nm}$, 2.84 V , 19 pA ; (c) $70 \text{ nm} \times 70 \text{ nm}$, 2.73 V , 27 pA , inset $8 \text{ nm} \times 4.5 \text{ nm}$; (d) $50 \text{ nm} \times 50 \text{ nm}$, 2.73 V , 27 pA , insets $4 \text{ nm} \times 4 \text{ nm}$; (e) $60 \text{ nm} \times 60 \text{ nm}$, -2.73 V , 23 pA ; (f) $50 \text{ nm} \times 50 \text{ nm}$, -2.78 V , 20 pA .

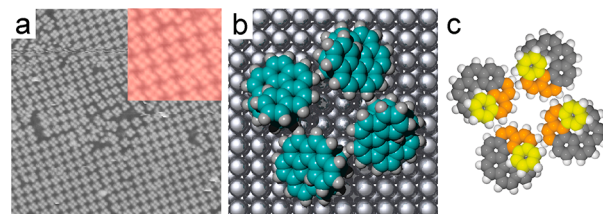


Figure 3. (a) STM image ($50 \text{ nm} \times 50 \text{ nm}$, 2.73 V , 20 pA , inset $4.1 \text{ nm} \times 4.1 \text{ nm}$) of a closed-packed *M*-[7]H monolayer on Ag(100). (b) Structure model of the *M*-[7]H quadruplet on Ag(100). (c) Homochiral *M*-quadruplet. The color sequence from yellow to orange to gray goes down counterclockwise.

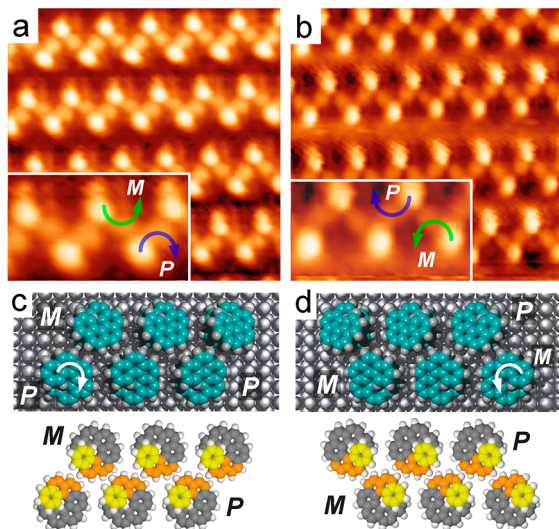


Figure 4. High resolution STM images with submolecular spatial resolution of zigzag rows formed by *rac*-[7]H on Ag(100) (a,b). The rows in both domains run along the same direction, but have mirror symmetry due to the *M-P* or *P-M* alignment of the molecules in a zigzag row ($8\text{ nm} \times 8\text{ nm}$; insets are cutouts at 167% of respective image, 1.89 V, 32 pA). The arrows highlight the clockwise or counterclockwise sequence of bright lobes, representing the sign of helicity of the molecules. (c,d) Structure models of both mirror domains taking the submolecular resolved features of the STM images into account. The handedness of single molecules is indicated by circular arrows (with the arrowhead being further below) and by a color code going down from yellow to orange to gray in a clockwise (*P*) or counterclockwise (*M*) fashion.

the absolute sense of helicity. At intermediate coverages there are many enantiomorphous zigzag rows adjacent to each other (Figure 2e, SI Figure S3), but this changes at higher coverage, when large single domains prevail. The submolecular resolution also suggests that in an *M-P* pair one enantiomer is rotated by 90° with respect to the other (Figure 4). The models shown in Figure 4c,d, in which all molecules occupy identical sites, take this aspect into account. Note that this structure exhibits glide plane symmetry (plane group *p2gg*). It is a (4 0, 0 7) structure with two molecules per unit cell.²³ This leads to a packing density per molecule of 117 \AA^2 , which is substantially lower than the 110.5 \AA^2 per molecule observed for the quadruplet structure of the pure enantiomers. A model with stronger overlap between the molecules (SI Figure S4) has only a slightly higher density than the enantiopure structure, but the enantiomers would be on different adsites.

Compared to the single components (bare metal surface and molecules in the gas phase) adsorption of the molecules leads to lower energy. As long as the intermolecular repulsion in the first layer does not match the adsorption energy, the lateral density of molecules will increase. Consequently, the principle of close-packing applies in particular to molecular 2D crystals, where compared to the molecules in the gas phase a higher 2D density (more molecules per unit area) leads overall to a larger gain of energy due to the interaction with the metal surface. Our experimental observations show, however, that—although lower in density—a heterochiral phase forms during growth of the molecular layer. That mere close-packing does not govern the 2D growth here is actually reflected by the fact that isolated heterochiral zigzag rows appear already at low coverage. These can grow longer, but homochiral structures larger than four

molecules are not observed. This is an indication that for four molecules homochiral structures are more stable, but for larger structures heterochiral zigzag chains are favored.

In order to compare the lateral binding energies within homochiral and heterochiral clusters, we performed Amber force field calculations for different cluster sizes. The interactions between molecule and surface were not taken into account, but the registry of the molecules on the surface was considered. That is, the molecules are forced into a certain configuration and are only partially allowed to relax. In particular the lower three C₆ rings were kept planar, because this configuration has been observed experimentally for [7]H on Cu(111).²⁴ Although this computational approach does not yield reliable absolute energy values, it very well allows comparison of different structures. This approach has been successful previously by predicting experimental observations made for [7]H on Cu(111).^{12,13}

The results for heterochiral dimers, tetramers, pentamers, and hexamers are listed in Table 1. The respective

Table 1. Binding Energies (kcal/mol) for Homochiral and Heterochiral Dimers, Tetramers, Pentamers, and Hexamers

composition	per cluster	per molecule
PM	43.03	21.52
PP	42.09	21.05
PPPM	82.01	20.50
PPPP	80.57	20.14
PMPMP	101.53	20.30
PPPPP	102.26	20.45
PMPMPM	120.68	20.11
PPPPPP	122.71	20.45

configurations are shown in the Supporting Information (SI Figure S5). The configurations of the homochiral quadruplet and heterochiral hexamer are also shown in Figures 3 and 4. The heterochiral tetramer is basically the four-molecule analogue of the hexamer. For the homochiral hexamer, two molecules were added to the most stable tetramer (SI Figure S5). For dimers and tetramers, the homochiral clusters are more stable; for larger structures such as a pentamer or hexamer a heterochiral composition is more favorable. The most stable homochiral structure is indeed the observed quadruplet.

These results explain perfectly the experimental observations. The lateral intermolecular interaction occurs under the limitation that the molecules prefer certain surface binding sites. Because more of the favored adsites can be occupied, a better match of a preferred molecular lattice with the substrate lattice results overall in a higher stability. On the other hand, a mismatch of the molecular lattice to the surface grid will introduce stress in any extended structure and lowers the stability. Once the stable homochiral quadruplet is formed, attaching more molecules to this structure is energetically not favorable. The possibility of sufficient lateral interaction by simultaneously occupying identical sites for the zigzag row, however, allows further growth without inducing stress in the molecular chain.

The fact that at higher coverages the homochiral quadruplets are not observed at all has to be due to their limited stability on this surface. As mentioned above, the homochiral quadruplet was previously observed for enantiopure [7]H on Au(111) and Cu(100) and for *rac*-[7]H on Cu(100). On Cu(100) all four

molecules in the unit cell occupy identical adsorption sites. The short interatomic distances on the closed-packed copper(111) and (100) surfaces of 2.55 Å match perfectly the C₆ ring center-to-center distance of polyaromatic molecules (SI Figure S6). Subsequently the quadruplet prevails even in the closed-packed monolayer of racemic [7]H on Cu(100). It is therefore one of the few examples of 2D conglomerate formation of helicenes.^{22,25}

Based on general symmetry arguments, it has been proposed that confinement at surfaces should favor conglomerate formation.^{26,27} Our study here shows that, at least for apolar molecules, the match of the footprint with the substrate surface plays a more important role. Because the monolayer or the nuclei at the surface serves as a template for further three-dimensional growth, the new insights into 2D crystallization reported here are useful for crystallization in general.

In conclusion, using scanning tunneling microscopy we could show that, although homochiral clusters of [7]H have a higher stability than the corresponding heterochiral clusters, only the latter are viable in order to grow larger nuclei on Ag(100). This favors then racemate formation over conglomerate formation.

ASSOCIATED CONTENT

Supporting Information

Long-range STM images of racemic and enantiopure 2D crystal structures, models for possible quadruplet arrangements and footprints as well as the arrangements of molecules for Amber force field cluster calculations. The Supporting Information is available free of charge on the ACS Publications website at DOI: 10.1021/jacs.5b02262.

AUTHOR INFORMATION

Corresponding Author

*E-mail: karl-heinz.ernst@empa.ch.

Notes

The authors declare no competing financial interest.

ACKNOWLEDGMENTS

Support by the Swiss National Science Foundation; project “Supramolecular Chiral Films”, and the University of Zurich Research Priority Program LightChEC is gratefully acknowledged. We thank Prof. Jack D. Dunitz for fruitful discussions.

REFERENCES

- (1) Hein, J. E.; Gherase, D.; Blackmond, D. G. *Top. Curr. Chem.* **2012**, *333*, 83–108.
- (2) Tamura, R.; Takahashi, H.; Fujimoto, D.; Ushio, T. *Top. Curr. Chem.* **2006**, *269*, 53–82.
- (3) Jacques, J.; Collet, A.; Wilen, S. H. *Enantiomers, Racemates, and Resolutions*; Krieger Pub. Co.: Malabar, FL, 1994.
- (4) Wallach, O. *Liebigs Ann. Chem.* **1895**, *279*, 119–143.
- (5) Brock, C. P.; Schweizer, W. B.; Dunitz, J. D. *J. Am. Chem. Soc.* **1991**, *113*, 9811–9820.
- (6) Dunitz, J. D.; Gavezzotti, A. *J. Phys. Chem. B* **2012**, *116*, 6740–6750.
- (7) Ernst, K.-H. *Phys. Status Solidi B* **2012**, *249*, 2057–2088.
- (8) Ward, M. D. *Nature* **2003**, *426*, 615–616.
- (9) Lemieux, R. P. *Acc. Chem. Res.* **2001**, *34*, 845–853.
- (10) Blaser, H.-U. *Tetrahedron: Asymmetry* **1991**, *2*, 843–866.
- (11) Seibel, J.; Parschau, M.; Ernst, K.-H. *J. Phys. Chem. C* **2014**, *118*, 29135–29141.
- (12) Fasel, R.; Parschau, M.; Ernst, K.-H. *Nature* **2006**, *439*, 449–452.
- (13) Parschau, M.; Fasel, R.; Ernst, K.-H. *Cryst. Growth Des.* **2008**, *8*, 1890–1896.
- (14) Seibel, J.; Zoppi, L.; Ernst, K.-H. *Chem. Commun. (Camb.)* **2014**, *50*, 8751–8753.
- (15) Böhringer, M.; Schneider, W. D.; Berndt, R. *Angew. Chem., Int. Ed.* **2000**, *39*, 792–795.
- (16) Cortés, R.; Mascaraque, A.; Schmidt-Weber, P.; Dil, H.; Kampen, T. U.; Horn, K. *Nano Lett.* **2008**, *8*, 4162–4167.
- (17) Vidal, F.; Delvigne, E.; Stepanow, S.; Lin, N.; Barth, J. V.; Kern, K. *J. Am. Chem. Soc.* **2005**, *127*, 10101–10106.
- (18) Mamdouh, W.; Dong, M.; Kelly, R. E. A.; Kantorovich, L. N.; Besenbacher, F. *J. Phys. Chem. B* **2007**, *111*, 12048–12052.
- (19) Gopakumar, T. G.; Matino, F.; Schwager, B.; Bannwarth, A.; Tuczek, F.; Berndt, R. *J. Phys. Chem. C* **2010**, *114*, 18247–18251.
- (20) Romer, S.; Behzadi, B.; Fasel, R.; Ernst, K.-H. *Chem.—Eur. J.* **2005**, *11*, 4149–4154.
- (21) Raval, R. *Chem. Soc. Rev.* **2009**, *38*, 707–721.
- (22) Seibel, J.; Allemann, O.; Siegel, J. S.; Ernst, K.-H. *J. Am. Chem. Soc.* **2013**, *135*, 7434–7437.
- (23) The (2×2) transformation matrix, linking the adsorbate lattice vectors (b_1, b_2) to the substrate lattice vectors (a_1, a_2) via $b_1 = m^{11}a_1 + m^{12}a_2$ and $b_2 = m^{21}a_1 + m^{22}a_2$, is written here in the form $(m^{11} \ m^{12}; m^{21} \ m^{22})$. See: Merz, L.; Ernst, K.-H. *Surf. Sci.* **2010**, *604*, 1049–1054.
- (24) Fasel, R.; Cossy, A.; Ernst, K.-H.; Baumberger, F.; Greber, T.; Osterwalder, J. *J. Chem. Phys.* **2001**, *115*, 1020–1027.
- (25) Stöhr, M.; Boz, S.; Schär, M.; Nguyen, M.-T.; Pignedoli, C. A.; Passerone, D.; Schweizer, W. B.; Thilgen, C.; Jung, T. A.; Diederich, F. *Angew. Chem., Int. Ed.* **2011**, *50*, 9982–9986.
- (26) Kuzmenko, I.; Weissbuch, I.; Gurovich, E.; Leiserowitz, L.; Lahav, M. *Chirality* **1998**, *10*, 415–424.
- (27) Pérez-García, L.; Amabilino, D. B. *Chem. Soc. Rev.* **2007**, *36*, 941–967.